Send Orders for Reprints to reprints@benthamscience.net

Medicinal Chemistry, **2019**, *15, Page Enation*

From Anti-infective Agents to Cancer Therapy: a Drug Repositioning Study Revealed a New Use for Nitrofuran Derivatives

Gabriella Ortore[a],*, Giulio Poli[a], Adriano Martinelli[a], Tiziano Tuccinardi[a], Flavio Rizzolio[b,c] and Isabella Caligiuri[c]

[a]*Department of Pharmacy, Pisa University, Pisa, Italy;* [b]*Department of Molecular Sciences and Nanosystems, Ca' Foscari University, Mestre, Italy;* [c]*Pathology Unit, Centro di Riferimento Oncologico (CRO) IRCCS, Aviano, Italy.*

Gabriella Ortore: gabriella.ortore@unipi.it

Giulio Poli: giulio.poli@unipi.it

Adriano Martinelli: adriano.martinelli@unipi.it

Tiziano Tuccinardi: tiziano.tuccinardi@unipi.it

Flavio Rizzolio: flavio.rizzolio@unive.it

Isabella Caligiuri: icaligiuri82@gmail.com

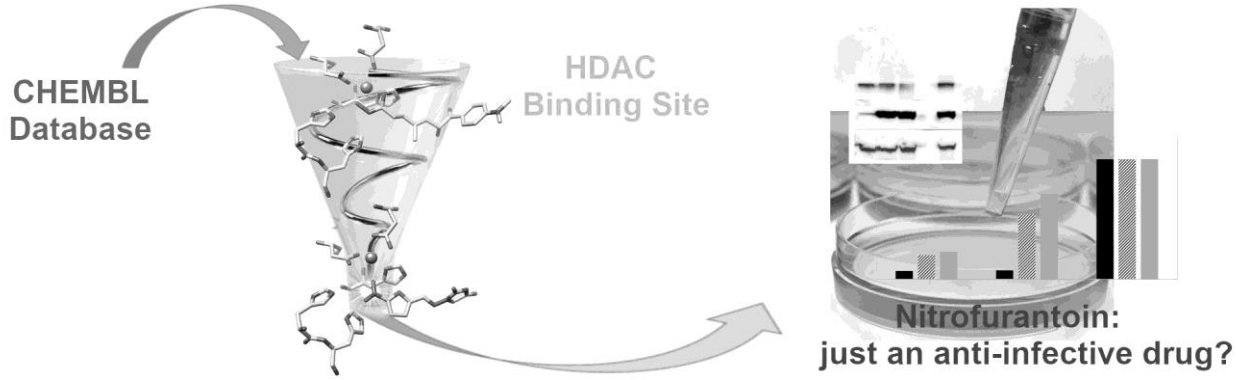

1573-4064 /19 $58.00+.00

ARTICLE TYPE

From Anti-infective Agents to Cancer Therapy: a Drug Repositioning Study Revealed a New Use for Nitrofuran Derivatives

Gabriella Ortore[a],*, Giulio Poli[a], Adriano Martinelli[a], Tiziano Tuccinardi[a], Flavio Rizzolio[b,c] and Isabella Caligiuri[c]

[a]Department of Pharmacy, Pisa University, Pisa, Italy; [b]Department of Molecular Sciences and Nanosystems, Ca' Foscari University, Mestre, Italy; [c]Pathology Unit, Centro di Riferimento Oncologico (CRO) IRCCS, Aviano, Italy.

ARTICLE HISTORY

Received:
Revised:
Accepted:

DOI:

Background: The progression of ovarian cancer seems to be related to HDAC1, HDAC3 and HDAC6 activity. A possible strategy for improving therapies for treating ovarian carcinoma, minimizing the preclinical screenings, is the repurposing of already approved pharmaceutical products as inhibitors of these enzymes.

Objective: This work was aimed to implement a computational strategy for identifying new HDAC inhibitors for ovarian carcinoma treatment among approved drugs.

Method: The CHEMBL database was used to construct training, test and decoys sets for performing and validating HDAC1, HDAC3 and HDAC6 3D-QSAR models obtained by using FLAP program. Docking and MD simulations were used in combination with the generated models to identify novel potential HDAC inhibitors. Cell Viability Assays and Western Blot Analyses were performed on normal and cancer cells for a direct evaluation of the anti-proliferative activity and an in vitro estimation of HDAC inhibition of the compounds selected through in silico screening.

Result: The best quantitative prediction was obtained for the HDAC6 3D-QSAR model. The screening of approved drugs highlighted a new potential use as HDAC inhibitors for some compounds, in particular nitrofuran derivatives, usually known for their antibacterial activity, and frequently used as antimicrobial adjuvant therapy in cancer treatment. Experimental evaluation of these derivatives highlighted a significant antiproliferative activity against cancer cell lines overexpressing HDAC6, and an increase in acetylated alpha-tubulin levels.

Conclusion: Experimental results support the hypothesis of a potential direct interaction of nitrofuran derivatives with HDACs. In addition to the possible repurposing of already approved drugs, this work suggests the nitro group as a new zinc binding group, able to interact with the catalytic zinc ion of HDACs.

Keywords: 3D-QSAR, docking, drug repurposing, HDAC inhibitors, nitrofurans, ovarian cancer, virtual screening.

1. INTRODUCTION

Histone deacetylases (HDACs) regulate many biological processes, by removing an acetyl group from histones. Their ability to bind many transcription factors influence cell proliferation, differentiation and development. [1] HDACs inhibition has multiple potential therapeutic applications, such as the treatment of neurological and inflammatory disorders, HIV, cystic fibrosis and cancer. [2-4] Different classes of histone deacetylase (HDAC) inhibitors endowed with anticancer activity are known among synthetic and natural compounds [5,6], and various representatives are involved in several preclinical experiments and clinical studies [7]. In particular, *in vitro* analysis performed on several ovarian carcinoma cell lines showed that knockdown of HDAC1 inhibits proliferation and tumorigenicity, knockdown of HDAC3 reduces cell migration and HDAC6 inhibition selectively promotes apoptosis of ARID1A-inactivated cells, supporting the use of HDAC6 inhibitors in the ovarian cancer treatment [8]. At present, two HDAC inhibitors completed clinical trials for the treatment of advanced ovarian epithelial cancer: vorinostat and belinostat [9,10]. Although both inhibitors have been considered pan-HDAC inhibitors, they showed a certain selectivity for HDAC1, HDAC3 and HDAC6 subtypes in enzyme inhibition fluorometric assays [11,12], thus suggesting a particular role of these three HDAC isoforms in the development and progression of ovarian cancer. In this context, we performed a computational study on HDACs, focusing our interest on HDAC1, HDAC3 and HDAC6. Our aim was the development of a computer-aided drug repurposing strategy focused on the identification of new anti-cancer compounds, based on the inhibition of HDAC1, HDAC3 and HDAC6, among drugs approved for different indications, thus suggesting novel therapeutic activities for some traditional medicinal compounds. Our work started with the development of 3D-QSAR models for the quantitative prediction of HDAC inhibitory activity [13,14], which were validated using hydroxamic inhibitors with known activities on HDAC1, HDAC3 and HDAC6. Good results were

*Address correspondence to this author at the Department of Pharmacy, University of Pisa, V. Bonanno, 6, Pisa, Italy; Tel/Fax: +39-050-2219572, +39 050 2210680; E-mails: gabriella.ortore@unipi.it

obtained in particular for the HDAC6 model, showing satisfying validation metrics. The three models were used to screen the approved drugs included in the CHEMBL database [15], identifying new compounds potentially able to stably bind HDACs. Molecular dynamics simulation, reflecting the time dependent conformational changes of protein-ligand complexes [16], confirmed the stability of our hit compounds in complex with HDAC6.

2. MATERIALS AND METHODS

2.1 *Docking Studies*

The available 13 crystal structures of all human HDACs co-crystallized with a hydroxamic inhibitor, with no missing significant sequence tracts, were selected from the Protein Data Bank (PDB) [17] for the docking procedure optimization (see Table S1). A cross-docking calculation in HDAC4 (PDB codes: 2VQM [18], 4CBT, 4CBY [19] and 5A2S [20]) and HDAC8 (PDB codes: 1T64, 1T69, 1VKG, [21] 3F0R and 3F07[22]), and a redocking in the unique crystal structure available for HDAC-1,2,6 and 7 subtypes (PDB codes: 5ICN [23], 4LXZ [24], 5EDU [25], 3C10 [26], respectively) were performed using all the fitness function available in the GOLD docking software [27] (ChemScore, GoldScore, ChemPLP and ASP). The ligands were extracted from the X-ray complexes and then subjected, after a minimization step, to a conformational search of 1,000 steps in a water environment (using the generalized-Born/surface-area model) by means of Macromodel [28] software to prevent the influence of the starting ligand geometry. The algorithm used was the Monte Carlo method with the MMFFs force field and a distance-dependent dielectric constant of 1.0. Missing hydrogens were added to the protein according to the predicted protonation state at the physiological pH, 7.0. Asn and Gln residues were absent in the range of interest for the direct contacts of docking; flip corrections were necessary only for the histidines involved in the zinc coordination, which were protonated in such a way to expose the lone pair towards the zinc atom. In view of testing the influence of a ZBG constraint on the disposition of the inhibitor tail, the docking calculations were performed taking the ligand completely free, or introducing a scaffold match constraint on the hydroxamate position deduced from the crystallographic ligand structures, with two different strength of the constraint: 5 as the default constraint and 0.5 as a light constraint. The region of interest for docking was defined in GOLD in such a manner that every protein contained all the residues within 10 Å from its co-crystallized ligand. The 'allow early termination' command was deactivated. All ligands were submitted to 40 Genetic Algorithm runs, clustering the output orientations using a RMSD cut-off of 1.5 Å. The metal coordination of the zinc ion was set in octahedral geometry, as in the crystallographic structures. The default GOLD parameters were used for all other settings. The resulting binding poses were compared with that observed in the X-ray crystal structure containing the ligands, through the calculation of the RMSD between them. The usual classification of results identifies the poses as best, medium and poorest fit as well as RMSD < 2Å, 2≤RMSD≤3 and RMSD > 3Å, respectively. Further docking calculations of CHEMBL ligands in the X-ray structures of HDAC1, HDAC3 and HDAC6 co-crystallized with hydroxamic acids (PDB codes 5ICN [23], 4A69 [29] and 5EDU [25], respectively) were carried out using the same procedure identified as the best through preliminary cross- and re-docking studies, by means of ASP as fitness function.

2.2. *3D-QSAR Modeling*

2.2.1. Training Set Definition

A CHEMBL database [15] query for detecting HDAC1, HDAC3 and HDAC6 known inhibitors with molecular weight within 250 and 400 g/mol (the common size of classical HDACs inhibitors) was run. The query results were further analyzed in view to filter only compounds whose IC_{50} data were known for all the three subtypes. The resulting 362 molecules were optimized through the Omega2 program of Openeye suite [30], setting the torsion driving parameters values of ewindow to 0.5 kcal/mol and rms to 2 Å. The lowest-energy conformer of each compound was subjected to docking into HDAC1, HDAC3, and HDAC6 using the above reported procedure. Due to the scaffold match constraint, all compounds lacking of at least two atoms shared with the hydroxamic moiety were rejected; the retained compounds were used as training set for generating a 3D-QSAR model. Five compounds among the best HDAC inhibitors (Vorinostat, Panobinostat, Dacinostat, Belinostat and Cudc-101) already FDA approved or included in clinical trials, were removed from the training set and successively used to validate the results.

2.2.2. 3D-QSAR model construction

The docking conformations of known HDACs inhibitors were used to construct a FLAP [9] database for each enzyme. FLAP is able to compare molecules using fingerprints. The fingerprints are derived from the GRID molecular interaction fields (MIFs) [31] and/or the GRID atom types, and are characterized as quadruplets of pharmacophoric features. The MIFs produced by the GRID force-field describe the type, strength and direction of the interactions owing to a molecule [32]. The quantitative examination of the MIF contributions to the activity for a set of aligned structures allows the construction of 3D-QSAR models [33]. In this context, the GOLD docking conformer for each ligand was imported in the FLAP database, setting to 0 the number of additional conformers to be generated. MIFs were then calculated using the acceptor (O), donor (N1), hydrophobic (DRY), and shape (H) probes, as implemented in FLAP, and using a grid resolution of 0.75Å. The interaction point energies were defined as independent variables, while the activity of the inhibitors, expressed as pIC_{50}, was set as the dependent variable. So, the docked dataset of compounds was used as training set to construct 3D-QSAR models, analyzing through Partial Least Squares (PLS) the combinations of descriptors that best explain the activity. The models were cross-validated using the LOO method, and analyzed in terms of R^2 and Q^2. The optimal number of latent variables was chosen for each model, and the prediction capability of the models against each inhibitor was examined.

2.2.3. External Set Definition, Screening and Validation

A CHEMBL database query for retrieving all approved drugs was run, downloading a database of up to 11000 compounds. The subsequent removal of non-small molecule drugs reduced the number to less than 6380 compounds. All these compounds were retrieved as sdf file and optimized through the Omega2 program of Openeye[30] suite, setting the torsion driving parameters values of ewindow to 0.5 kcal/mol

and rms to 2 Å. The lowest-energy conformer of each compound was subjected to docking into HDAC1, HDAC3, and HDAC6 using the above reported procedure. The retained compounds in the resulting docking poses (filtered by the scaffold match constraint) were used as an enriched dataset for a 3D-QSAR screening. In fact, among the 88 drugs survived to the scaffold match constraint, 9 compounds were known actives ligands of HDAC1, HDAC3 and HDAC6, one compound was selectively active against HDAC6 and inactive against HDAC1 and HDAC3, while the remaining 78 compounds could be considered as "decoys" (see Table S2 and Results and Discussion for more details). The known HDAC ligands were used to validate the model and the potential HDAC inhibitory activity of the decoys was predicted through our 3D-QSAR model. The screening results were assessed using the enrichment factor (EF) and the receiver operator characteristic (ROC) curve profile [14]. The EF measures the enrichment of the method compared with random selection:

$$EF = [tp/(tp + fn)](NCtot/NC)$$

where tp is the number of known active ligands retrieved (true positives); fn is the number of known active ligands discarded during the VS filtering (false negatives); NCtot is the total number of compounds of the database; NC is the total number of molecules obtained by the VS protocol. The ROC curve profile graphically emphasizes the performance of each model on enrichment, suggests if early recognition has been achieved by the three models and which fraction of the molecular dataset corresponds to the best EF. The hits were analyzed in view of their structure, therapeutic use and activity on known targets, being not usual "decoys" but actual drugs (see Table 2). The performance of the screening, in this case, could also be influenced by the presence of true active compounds such as remetinostat, whose inhibition values were not reported. The hits common to HDAC1, HDAC3 and HDAC6 were evaluated for choosing the best candidates to submit for biological testing.

2.3. *Molecular Dynamics Simulations*

Nitrofurazone and nitrofurantoin were subjected to molecular dynamics in HDAC1, HDAC3 and HDAC6. Complexes were derived from their best docking pose within the enzyme binding and the simulation was performed using AMBER 14 [34]. The complexes were placed in a rectangular parallelepiped water-box, an explicit solvent model for water (TIP3P) was used; the complexes were solvated with a 10 Å water cap. Sodium ions were added as counterions to neutralize the system. Prior to MD simulations, three steps of minimization were carried out, first optimizing the solvent, then relaxing the complex and the ligand. Particle mesh Ewald electrostatics and periodic boundary conditions were used in the simulation. The MD trajectories were run using the minimized structures as the starting conformations. The time step of the simulations was 2.0 fs with a cutoff of 10 Å for the non-bonded interaction, and SHAKE was employed to keep all bonds involving hydrogen atoms rigid. Constant-volume periodic boundary MD was carried out for 500 ps, during which the temperature was raised from 0 to 300 K. Then, 9.5 ns of constant-pressure periodic boundary MD was carried out at 300 K by using the Langevin thermostat to maintain the temperature of our system constant, constraining all the α carbons, catalytic Zn and ligand with 10 kcal of harmonic force constant in the first 1600 ps; then the ligand was relaxed and the last 6.3 ns of simulation were performed without any constraint. General Amber force field (GAFF) parameters were assigned to the ligands, while partial charges were calculated using the AM1-BCC method. The MD trajectories were analyzed by using the MD Movie tool of Chimera, and through the cpptraj module of Amber14 [35] (see Fig S1).

2.4. *Cell Viability Assay*

OVCAR3, MDA-231 and MRC5 were maintained at 37 °C in a humidified atmosphere containing 5% CO_2 according to the supplier (LGC Standards, Milan, Italy, EU). Normal (1.5×10^4) and cancer (5×10^2) cell lines were plated in 96-well culture plates. The day after seeding, vehicle or compounds were added at different concentrations to the medium. The compounds Nitrofurantoin, Nitrofurazone (both from Sigma-Aldrich, with Purity >98%) and Ricolinostat (from Selleckchem, with 99.89% purity) were solubilized in DMSO and added to the cell culture at a concentration ranging from 200 to 0.02 μM. Cell viability was measured with Cell Titer-Glo (G7571) after 96 h according to the supplier (Promega, Madison, WI, US) with a Tecan M1000 instrument. IC_{50} values were calculated from logistical dose response curves [36]. Averages and standard deviations were obtained from triplicate experiments.

2.5. *Western Blot Analysis*

Cancer cells were pelleted and resuspended into RIPA buffer (10mM Tris-Cl (pH 8.0), 1% NP-40, 0.1% sodium deoxycholate, 0.1% SDS, 140 mM NaCl.) supplemented with a protease inhibitor mixture (Complete-EDTA, Roche, Switzerland) for protein extraction [37]. The amount of total proteins was measured with the Bradford method and 50 μg of proteins were loaded and run on a 4-12% TruPAGE™ Precast Gel utilizing the TruPAGE™ TEA-Tricine SDS Running Buffer (Sigma-Aldrich, St. Louis, MO, US). The proteins were separated for approximately one hour at 100 V. After electrophoresis, the proteins were transferred on a nitrocellulose membrane (Whatman International Ltd., UK), utilizing a TruPAGE™ Transfer Buffer (Sigma-Aldrich, St. Louis, MO, US) with 20% methanol for 1 hour at 100 V and 1 hour at 70 V in ice. The membranes were blocked with 5% (w/v) skim milk in Tris-buffered saline Tween 20 solution (TBS-T) for 30 minutes and incubated overnight at 4 °C on a shaker with HDAC6 (Proteintech Group, Rosemont, IL, US; 12834-1-AP), α-Tubulin (acetyl k40) (Abcam, Cambridge, UK; ab179484) and HSP70 (Santa Cruz, CA, US; sc-24) primary antibodies in 5% skim milk TBS-T [38]. The membranes were washed 3 times in agitation with TBST for 5 minutes, incubated for 1 hour with secondary antibodies in 5% milk TBS-T at RT, developed with enhanced chemiluminescence (ECL) solution, and visualized with ChemiDoc Imager instrument (Bio-Rad Laboratories, CA, US).

3. RESULTS AND DISCUSSION

3.1. *Docking reliability studies*

In order to evaluate the best docking procedure for simulating the binding of different compounds into HDAC1, 3 and 6, a self- and cross-docking evaluations [39] were carried out by considering all crystal structures of human HDACs co-crystallized with a hydroxamic inhibitor (see Table S1 in the Supporting Information), deposited in Protein Data Bank. For

HDAC4 and HDAC8 a cross-docking evaluation was possible (due to the presence of four ligand-protein complexes for each subtype) whereas, due to the limited number of ligand-protein complexes, for HDAC1, 2, 6 and 7 a self-docking analysis was carried out. GOLD docking software was used applying ASP, ChemPLP, ChemScore and GoldScore fitness scoring functions [40] and considering also the possibility of applying a scaffold match constraint on the hydroxamate moiety deduced from the crystallographic ligand structures [41]. As shown in Fig. 1, measuring the root-mean-square deviation (RMSD) of the position of the docked ligands with respect to their experimentally determined disposition, the use of the ASP scoring function applying the scaffold match constraint was the procedure that showed the best results, with an average RMSD of 3.2 Å, and was therefore applied for further calculations.

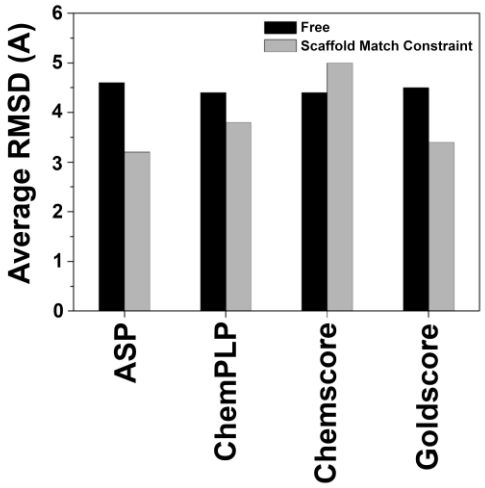

Fig. 1: RMSD results of cross-docking and self-docking analyses using the four GOLD docking procedures, in presence and absence of the scaffold match constraint.

3.2. *3D-QSAR Modeling*

The CHEMBL web server [15] was inspected to obtain structures and activity data of molecules already tested against HDAC1, HDAC3 and HDAC6. The study was restricted to compounds with molecular weights between 250 and 400 g/mol. Among the 1718 compounds with known activities on HDAC1, 428 on HDAC3 and 954 on HDAC6, just the 362 molecules which were tested against all three subtypes were considered. Among them, the five HDAC inhibitors that were in different stages of clinical trials (Vorinostat, Panobinostat, Dacinostat, Belinostat and Cudc-101) were removed from this set and subsequently used for enriching an external database. The 357 compounds were submitted to docking studies into the X-ray structures of the three HDAC isoforms (PDB codes 5ICN [23], 4A69 [29] and 5EDU [25] for HDAC1, HDAC3 and HDAC6, respectively) employing the ASP fitness scoring function. By applying the scaffold match constraint, all compounds matching less than two out of the four atoms of the hydroxamic moiety of the HDAC co-crystallized ligands were discarded. As a result, only 217 ligands survived the docking step. These compounds were then aligned and used as a training set for generating 3D-QSAR models through FLAP program (Fingerprints for Ligands And Proteins) [13]. The activities extrapolated from the CHEMBL database were imported in FLAP as pIC_{50} and this step produced some small fluctuation in the training set composition. In fact, some activities were not reported in the CHEMBL database as precise values and this required the elimination of 10 compounds from the HDAC1 training set and 14 from the HDAC3 one, thus resulting in 193 compounds. The software FLAP generated the Molecular Interaction Fields (MIFs) for the training set ligands using default probes; subsequently, the obtained MIFs were correlated with the corresponding ligands' activities through a PLS calculation [42]. In Table 1, the statistical results in terms of correlation coefficients relative to a Leave One Out (LOO) cross validation are reported. The results were adequate to the system environment. In fact, the variability in the training set was very high and the binding site location allowed a very different disposition of docked compounds on the protein surface, in agreement with the experimental structures available through X-ray crystallography. In this context, the results showed a correlation higher than 0.9 and the cross-validation term indicated a good prediction ($Q^2 > 0.5$). In particular, the best model was generated for the most populated training set of HDAC6, reaching a Q^2 value of 0.67.

Table 1. Statistical results of the 3D-QSAR calculation.

	HDAC1	**HDAC3**	**HDAC6**
R^2	0.91	0.90	0.94
Q^2	0.56	0.54	0.67
SDEP ext	0.82	0.69	0.57

The good predictivity of the three HDAC models allowed their use for further calculations in virtual screening or activity predictions.

3.3. *External Evaluation and Virtual Screening Study*

A new dataset of compounds belonging to ChEMBL database was created for validating the 3D-QSAR models and to search for possible HDAC inhibitors among already known drugs. The dataset of approved drugs was used for the validation of our models as an enriched database in which known HDAC inhibitors were considered as true actives and all other compounds, with biological activity against other targets, were considered as decoys (see the Material and methods section in the Supporting Information). A CHEMBL query of approved small-molecule drugs retrieved a database of 6380 compounds that were subjected to the docking protocol already described. A docking result could be generated only for the 88 molecules that sufficiently matched the hydroxamate scaffold and thus passed the docking restraint, rarely with unfavorable steric clash forced by the constraint (e.g. Filanesib in HDAC1). The best docking poses of these compounds (some representative results, restricted to most interesting non-hydroxamic compounds, are reported in Figs. S2-S4) were used as an external test set for validating the three models, which also included 10 known HDAC inhibitors. Among these, Cudc-101 [43], Dacinostat [44], Panobinostat [45], Vorinostat [44] and Belinostat [45] were previously removed from the training set, being the best candidates as external test compounds due to their overcoming of many clinical trials. Moreover, Ricolinostat [46], which completed two clinical trials on multiple

myeloma patients and on healthy subjects [47], was not comprised in the training set because of its molecular weight of 434 g/mol. For these six reference ligands, IC_{50} values of HDAC1, HDAC3 and HADC6 were reported and their activities could be thus predicted quantitatively through our models. The remaining four known HDAC inhibitors included in our test set were not used for the training set because they lacked of IC_{50} data annotations. In particular, for Quisinostat and Abexinostat K_i values of inhibition were reported [48], indicating good activity especially against HDAC1 and lesser potency on HDAC6, but these values could not be used in the quantitative prediction due to lack of homogeneity among data. For Nicoxamat [49] only the activity/inactivity in a Western blot analysis was reported. Finally, no details about the selectivity profile of Remetinostat were known, in spite of its efficacy in reducing cutaneous T-cell lymphoma skin lesions in the Phase II trial [50]. Although Remetinostat was predicted to interact with HDAC8, HDAC6 and HDAC3 at 1 μM concentration with full score [15], we had no precise experimental information about its effect on these HDAC isoforms and its activity on HDAC1. However, we could still consider it as a reference inhibitor and check the behavior of this compound during the screening. Therefore, our external database consisted of 78 decoys and 10 known inhibitors.

The database was screened through the HDAC1, HDAC3 and HDAC6 models; the predicted activities of all screened compounds are reported in Table S2. By just looking at the top-ranked ligands, it would seem that the HDAC3 model was the best in qualitatively discriminating actives from decoys, since 7 out of the first 10 compounds were known HDAC inhibitors. Nevertheless, the evaluation in terms of global quantitative prediction showed different results: the SDEP calculated on the six known ligands was 0.82 for HDAC1, 0.69 for HDAC3 and 0.57 for HDAC6, showing a better quantitative prediction for HDAC6 inhibition (see Table 1).

An evaluation of the screening power of our model was performed through the ROC plots reported in Fig. 2 and calculating the enrichment factor (EF). For HDAC3, the ROC plot showed a classical behavior reaching the plateau after 25% of database filtration, corresponding to an EF value of 3.5. For HDAC6, the screening had weak efficiency, although better than a random performance, reaching the plateau after 40% of database filtration, with an EF of 2.2. Very peculiar was the trend of HDAC1 screening: 30 decoys were ranked between the 3rd and 4th active compound, causing a stationary trend of the ROC plot, which increased its slope in the 40 - 45% range of database filtration. The definitive plateau of the curve was reached around 50% of the ranked database, corresponding to an EF value of 1.6. In addition to these parameters, we checked the early-filtered decoys for better analyzing the performance of these models. For example, Remetinostat was considered an early-filtered decoy for HDAC1 and HDAC3, but it was an actual HDAC inhibitor without information about subtype activity [50]. Bufexamac, an early-filtered decoy for HDAC6 model, was found to exhibit HDAC activity with moderate selectivity for HDAC6 [51], while Benurestat was a urease inhibitor [52], but was predicted as HDAC1 and HDAC6 inhibitor in the CHEMBL target predictions section. Some early-filtered decoys were MMP inhibitors (Marimastat, Apratastat, Prinomastat), which share with HDAC inhibitors the zinc binding groups [53]. Interestingly, a dual HDACs/MMPs inhibition was recently suggested as a mechanism to improve the response rate in treating tumors [54], and this would inspire interesting further studies on these decoys in a separate context. Overall, all three models were able to discriminate actives from decoys; despite the lower EF registered for the HDAC1 model, this performed significantly better than random selection and was able to early-filter decoys that are most likely to be HDAC inhibitors.

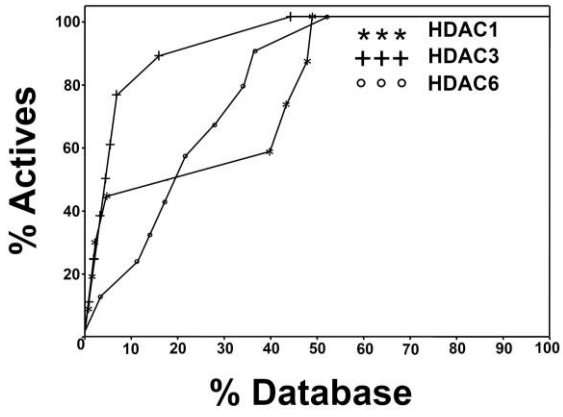

Fig. 2: ROC curves of the VS. FLAP receptor-based filtering results obtained for the CHEMBL drugs database vs known HDACs inhibitors

Hit compounds that survived the screening filter in HDAC1, HDAC3 and HDAC6 models (see Table S2) were analyzed to further assess their potential HDAC inhibition activity. Among these compounds, nine were predicted as potential active against all three analyzed HDACs. This requirement, the surviving in all three HDACs, in addition to FLAP prediction, allowed to discard potential false positives like Filanesib. As shown in Table 2, hits comprised Ricolinostat, Cudc-101, Dacinostat and Panobinostat, which are known HDACs inhibitors, and four nitrofuran derivatives (Nidroxyzone, Nifurdazil, Nifurtoinol and Nitrofurantoin). The most evident result of this work was that the nitro group, not emerged from previous large-scale studies [55], was highlighted as a possible ZBG for HDACs. Actually, some preliminary evidence of inhibitory activity against other metalloenzymes was already shown for Nifursol and Nitrofurantoin: on DRUGMATRIX database [56], an inhibition of the enzymatic activity (below 50%) of CA (carbonic anhydrase) II, MMP (metalloproteinase) 1, MMP9 and ACE (angiotensin-converting-enzyme inhibitor) was reported for these compounds, tested at a concentration of 10 μM. However, no evidence of HDACs inhibitory activity has ever been reported for these compounds. An ADMET [57] properties evaluation of these compounds has been performed using the SwissADME website. No Lipinski rule violations, no CYP inhibition or ability to be a substrate of Pgp have been detected for all nitrofuran derivatives. The commercial availability and the structural similarity of these four compounds were analyzed: Nidroxyzone, presenting a free hydrazinecarboxamide moiety instead of the cyclic analogues of the other hits, was not available in stock. For this reason, we checked the most similar candidates among the first discarded decoys. Nifurethazone, predicted as the best potential HDAC6 inhibitor but not shared with HDAC1 and HDAC3, was also not available. Nitrofurazone, which passed the screening of HDAC1 and HDAC3 models, and was predicted to be slightly less active with respect to Nicoxamat

against HDAC6, was available. Therefore, we analyzed the stability of its predicted binding mode into HDAC1, HDAC3 and HDAC6 using molecular dynamics (MD) simulations; the same analysis was also performed for Nitrofurantoin, the only common hit available in stock that shared 60% of Tanimoto similarity with Nifurdazil and Nifurtoinol.

Table 2. VS hits and their common therapeutic use.

Hits	Structure	Activity [a]
Ricolinostat	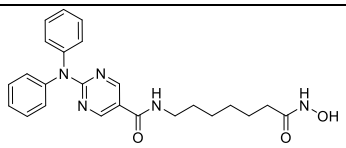	Epigenetic regulator
Benurestat	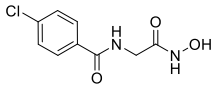	Urease inhibitor
Cudc-101	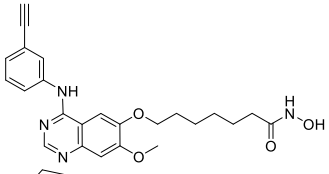	Epigenetic regulator
Dacinostat	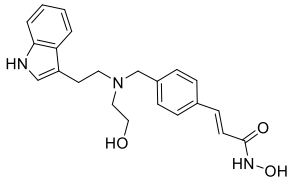	Epigenetic regulator
Panobinostat	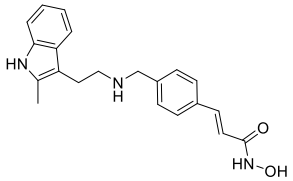	Epigenetic regulator
Nidroxyzone	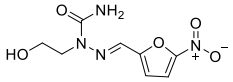	Anti-infective
Nifurdazil	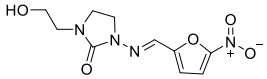	Anti-infective
Nifurtoinol	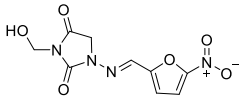	Anti-infective
Nitrofurantoin	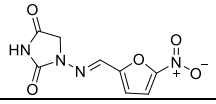	Anti-infective

[a] Ref. [15]

3.4. *Molecular Dynamics Evaluation*

Molecular dynamics simulation provides several conformations of a protein to sample the thermodynamically viable flexibility of residues [16]. This is very helpful in a variety of application, such as model refinement, allosteric regulation, identification of transition states in a complexation [58], homology modelling [59,60] or assessment of the stability of docking complexes [61]. Nitrofurazone and Nitrofurantoin in complex with HDAC1, HDAC3 and HDAC6, were studied through 10 ns of molecular dynamics simulation and the reliability of their predicted binding modes were analyzed. As reported in Fig. S1, all complexes showed a remarkable stability during the simulation, with only a small fluctuation of the protein α carbons in terms of RMSD from the starting coordinates (dark RMSD plot). The docking pose of Nitrofurantoin was well retained in HDAC6: just a deviation of 2.0 Å was registered for the ligand before reaching the equilibrium pose. In HDAC1 (Figs. 3a and S5a) the whole zinc coordination environment was subjected to a shift toward the inner part of the protein, highlighted by ligand RMSD values of about 5.0 Å after 4 ns of simulation. The zinc coordination was anyway guaranteed in both cases by a distance O_2N–Zn of 2.3 and 2.5 Å, respectively (see Figs. 3c and 3a, S5c and S5a). In HDAC3, the rotation of the furan ring moved the nitro group of the ligand away from the metal ion (see Figs. 3b and S5b). Therefore, the ligand lost their interactions with zinc, although it occupied the binding site. Nitrofurazone was less stable during the simulation; in HDAC1 and HDAC3 complexes the O_2N–Zn distance

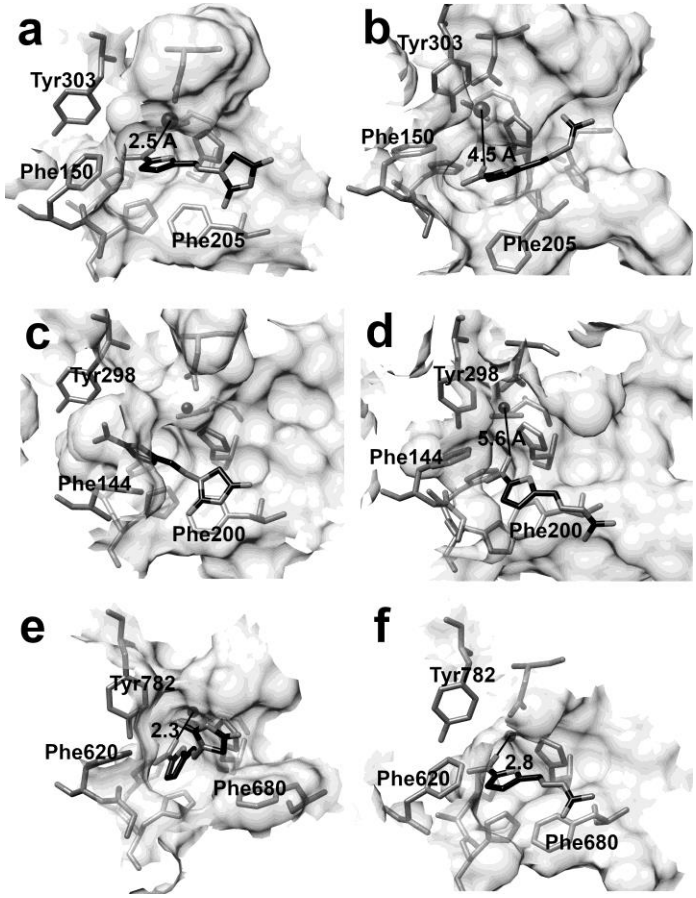

Fig. 3: Disposition after MD simulations of Nitrofurantoin in HDAC1 (a), HDAC3 (c) and HDAC6 (e), and of Nitrofurazone in HDAC1 (b), HDAC3 (d) and HDAC6 (f).

reached a value of about 6 Å, nevertheless values of 4.5 and 5.6 Å were measured in the minimized average structure (Figs. 3d and 3e, S5d and S5e). In HDAC6 the system showed a considerable fluctuation of both O_2N–Zn distance and ligand RMSD, around an average value of 3.0 Å; nevertheless, the ligand maintained its binding mode and its interactions with the zinc ion. In fact, the minimized average structure of Nitrofurazone in complex with HDAC6 (Figs. 3f and S5f) showed a distance between the oxygen and the zinc ion corresponding to 2.8 Å, which could be considered as the threshold distance for metal coordination. Differently, the minimized average structure of nitrofurantoin in complex with HDAC6 highlighted a more stable zinc coordination

complex with an oxygen of the ligand nitro group interacting with the zinc ion at a distance of 2.3 Å and the other nitro oxygen forming an H-bond with His610, thus further stabilizing the ligand-protein complex.

Compared to classical hydroxamate inhibitors, which use carbonyl and hydroxamate oxygen atoms for zinc coordination, the nitro group loses one coordination point. The interaction between Asp742 and zinc becomes a bidentate-like coordination and His610 is still involved in the inhibitor stabilization. A similar role of the nitro group was already reported in the zinc coordination of 2-benzyl-3-nitropropanoic acid in the carboxypeptidase A [62] (PDB code 2RFH). With regards to the nitrofurantoin tail, it was highly stabilized on the binding pocket surface through a strong stacking interaction formed among the ligand imidazolidinedione moiety (well-known to establish such interactions) [63], Phe620 and Phe680 (Fig. 3c). These interactions surely contributed to stabilize the binding mode of nitrofurantoin during the MD simulation. The metal coordination in HDAC6–nitrofurazone complex was more susceptible to some MD fluctuation, which strongly depended on the tail plasticity of the inhibitor. The polar and water exposed semicarbazone group was highly flexible during the simulation and allowed a significant shift in the ligand position. During the MD simulation, the nitro group of nitrofurazone competed with His610 for zinc coordination, reaching a total displacement after about 7 ns of MD. After this peak, the inhibitor returned to the binding site and restored the coordination, keeping it for next 2 ns (Fig. S1). The fluctuation could be an indication of the poor stability of the system, but the inhibitor propensity to restore the coordination after leaving the binding site suggested the presence of strong interactions with HDAC6 residues and catalytic zinc.

3.5. *Western Blot Analysis and Cell Viability Test*

Based on the MD results, nitrofurantoin and nitrofurazone were tested to evaluate their HDAC6 inhibitory activity. The classical biochemical assay for measuring HDAC6 activity is based on a fluorogenic substrate, which produces a fluorophore that can be measured using a fluorescence reader. Both nitrofurantoin and nitrofurazone are yellow powders that can absorb light in the region of detection and affect the readout. Therefore, fluorescence-based assays could not be used to test our hits for HDAC6 inhibitory activity. For this reason, the two compounds were directly evaluated for their anticancer activities on ovarian (OVCAR-3), breast (MDA-231) cancer and normal MRC5 cells, using ricolinostat (a highly selective HDAC6 inhibitor) as a positive control. Modest cytotoxicity was already registered for nitrofurantoin, used as a reference compound, on some human cancer cell lines in studying cytotoxic and antibacterial activities of new heteroaryl-acrylonitriles [64]. More recently, because nitrofurans are a class of compounds that is poorly explored with respect to their anticancer potential, Andrade et al. investigated the anticancer effects on HL-60 leukemia cells of a nitrofurantoin derivative, n-pentyl-nitrofurantoin (NFP), which resulted in about 4 fold more cytotoxic against HL-60 leukemia cells than against normal cells [65]. Also nifuroxazide produced an effective decrease in the viability of multiple myeloma cells, due to inhibition of STAT3 [66], which was successively discovered to be modulated by HDAC inhibition [67]. In order to test the anticancer activities in cell lines that express HDAC6 high protein level, a western blot analysis was carried out. As shown in Fig. 4, HDAC6 protein is abundant in all cancer cell lines tested.

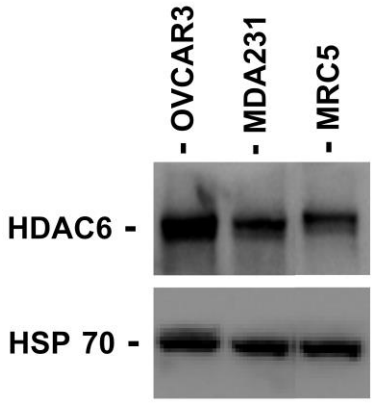

Fig. 4: Protein expression of HDAC6 in different cancer cell lines. Heat shock protein (HSP)70 antibody was utilized as control.

Nitrofurantoin caused a significant inhibition of cell viability, with IC_{50} values of 21.1 and 54.2 μM for the OVCAR-3 and MDA-231 cell lines, respectively, whereas it proved to be inactive against noncancerous human fibroblast lung cells MRC5 (p-values << 0.001 for both cancer cell lines). Same trend, but slightly weaker activities, were registered for nitrofurazone, in agreement with the lower stability of its HDAC6 complex compared to nitrofurantoin. The results showed an activity just three times weaker than ricolinostat in OVCAR-3 cells (Fig. 5), which could be consistent with the weaker zinc coordination of the nitro group with respect to the hydroxamate group.

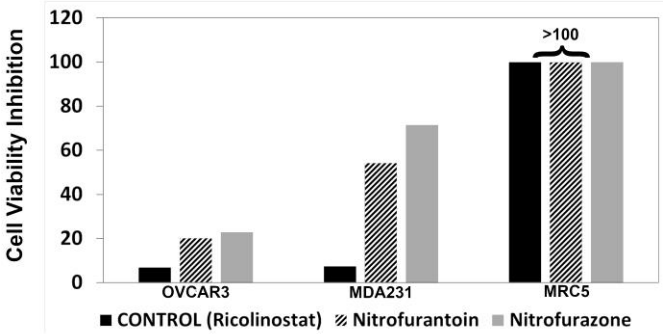

Fig. 5: Cell growth inhibitory activities (IC_{50}) of nitrofurantoin and nitrofurazone.

The optical interference precluded the application of fluorescence-based methods, which could provide clear and definitive information on the affinity of nitrofuran derivatives for HDAC6. With the aim to provide further data to confirm this hypothesis, OVCAR3 cell protein extracts were prepared and the relative levels of acetylated alpha-tubulin (HDAC6's target) were determined by Western blot using an anti–acetylated tubulin antibody. Although no major changes in protein expression were observed for HDAC6 in the presence of Nitrofurazone and Ricolinostat, there is a reduction of HDAC6 protein level in the presence of Nitrofurantoin (Fig. 6). For all the compounds, the western blot analysis demonstrates an increase in acetylated alpha-tubulin in OVCAR3 cells. This result confirms the ability of Nitrofurantoin and Nitrofurazone to be novel substrates for HDAC6. The PLS pseudocoefficient plot of the 3D-QSAR

model (see Fig. S6) appears to mainly correlate the activity with the descriptors derived from the DRY and N1 MIFs, which are related to the furan and carbonyl moieties of Nitrofurantoin, respectively.

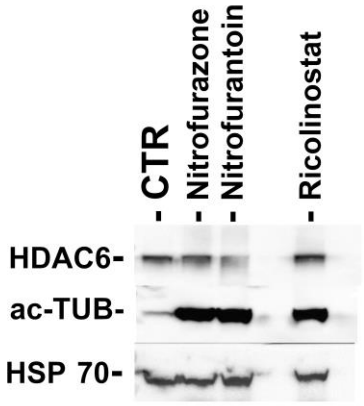

Fig. 6: Effect of nitrofurazone, nitrofurantoin and ricolinostat on the expression of HDAC6, acetylated alpha-tubulin in OVCAR3 cells. Heat shock protein (HSP)70 antibody was utilized as control.

The ingrained interaction between nitrofuran derivatives and the catalytic zinc ion that emerged in this study represents a first attempt to use nitro groups as ZBGs in the design of novel HDAC inhibitors. Furthermore, the cellular growth reduction observed for the two compounds in cancer cell lines overexpressing HDAC6, and the increased expression of acetylated alpha-tubulin in the presence of both compounds, corroborated the possible drug repositioning of well-known nitrofuran derivatives as HDAC6 inhibitors, working for ameliorating their pharmacokinetic profile. The inactivity of the compounds against noncancerous human cells suggested their potential applications in anticancer therapy, not correlated to their anti-infective function.

4. CONCLUSION

In the present work, a docking/3D-QSAR-based virtual screening approach was developed with the aim of identifying new antitumor agents, potentially active in ovarian cancer treatment, among drugs already registered for other indications. The applied computational workflow suggested as potential HDAC1/HDAC3/HDAC6 inhibitors nitrofuran derivatives, known as anti-infective drugs. Among these, nitrofurantoin and nitrofurazone also showed good stability in complex with HDAC6, based on MD simulations studies, maintaining the coordination with the catalytic zinc ion. The role of the nitro group as ZBG was occasionally reported for other enzymes [62], but not for HDACs. In addition to the potential identification of a new ZBG, this study suggested a new secondary role of nitrofuran derivatives as HDAC6 inhibitors. The experimental studies herein reported, revealed significant anticancer activity against cancer cell lines overexpressing HDAC6, corroborating a possible direct involvement in anticancer activity. Furthermore, the increased expression of acetylated alpha-tubulin in OVCAR3 cells in the presence of our nitrofuran derivatives is coherent with the inhibition of HDAC6, suggesting a further repurposing of these anti-infective drugs. The inactivity of nitrofurantoin against noncancerous human cells encouraged potential applications in anticancer therapy.

List of Abbreviations: EF, Enrichment Factor; HDAC, Histone Deacetylase; LOO, Leave One Out; MD, Molecular Dynamics; MIF, Molecular Interaction Field; MMP, Matrix Metalloproteinase; PDB, Protein Data Bank; PLS, Partial Least Squares; RMSD, root mean square deviation; R^2, correlation coefficient; SAR, Structure−activity relationship; SDEP, Standard Deviation of prediction errors; VS, Virtual Screening; ZBG, Zinc Binding Group.

ETHICS APPROVAL AND CONSENT TO PARTICIPATE

Not applicable.

HUMAN AND ANIMAL RIGHTS

No Animals/Humans were used in this research.

CONSENT FOR PUBLICATION

Not applicable.

AVAILABILITY OF DATA AND MATERIALS

Not applicable.

FUNDING

This project received support from MIUR (the Italian Ministry of Education, Universities and Research).

CONFLICT OF INTEREST

The authors declare no conflict of interest, financial or otherwise.

REFERENCES

[1] Wiech, N.; Fisher, J.; Helquist, P.; Wiest, O. Inhibition of Histone Deacetylases: A Pharmacological Approach to the Treatment of Non-Cancer Disorders. *Curr. Top. Med. Chem.*, **2009**, *9* [3], 257–271.

[2] Shukla, S.; Tekwani, B.L. Histone Deacetylases Inhibitors in Neurodegenerative Diseases, Neuroprotection and Neuronal Differentiation. *Front. Pharmacol.*, **2020**, *11*, 537.

[3] Shakespear, M.R.; Halili, M.A.; Irvine, K.M.; Fairlie, D.P.; Sweet, M. J. Histone Deacetylases as Regulators of Inflammation and Immunity. *Trends Immunol.*, **2011**, *32* [7], 335–343.

[4] Divsalar, D.N.; Simoben, C.V.; Schonhofer, C.; Richard, K.; Sippl, W.; Ntie-Kang, F.; Tietjen, I. Novel Histone Deacetylase Inhibitors and HIV-1 Latency-Reversing Agents Identified by Large-Scale Virtual Screening. *Front. Pharmacol.*, **2020**, *11*.

[5] Eckschlager, T.; Plch, J.; Stiborova, M.; Hrabeta, J. Histone Deacetylase Inhibitors as Anticancer Drugs. *International Journal of Molecular Sciences*. 2017.

[6] Poli, G.; Di Fabio, R.; Ferrante, L.; Summa, V.; Botta, M. Largazole Analogues as Histone Deacetylase Inhibitors and Anticancer Agents: An Overview of Structure–Activity Relationships. *ChemMedChem*, **2017**, *12* [23], 1917–1926.

[7] Mottamal, M.; Zheng, S.; Huang, T.; Wang, G. Histone Deacetylase Inhibitors in Clinical Studies as Templates for New Anticancer Agents. *Molecules*, **2015**, *20* [3], 3898–3941.

[8] Altucci, L. A Key HDAC6 Dependency of ARID1A-

Mutated Ovarian Cancer. *Nat. Cell Biol.*, **2017**, *19* [8], 889–890.

[9] National Cancer Institute. Vorinostat in Treating Patients With Recurrent or Persistent Ovarian Epithelial or Primary Peritoneal Cavity Cancer. In: ClinicalTrials.gov [Internet]. Bethesda (MD): U.S. National Library of Medicine, **2000**. Available from: https://clinicaltrials.gov/ct2/show/NCT00132067.

[10] National Cancer Institute. Belinostat in Treating Patients With Advanced Ovarian Epithelial Cancer, Primary Peritoneal Cancer, or Fallopian Tube Cancer or Ovarian Low Malignant Potential Tumors. In: ClinicalTrials.gov [Internet]. Bethesda (MD): U.S. National Library of Medicine, **2000**. Available from: https://clinicaltrials.gov/ct2/show/NCT00301756.

[11] Jones, P.; Altamura, S.; De Francesco, R.; Gallinari, P.; Lahm, A.; Neddermann, P.; Rowley, M.; Serafini, S.; Steinkühler, C. Probing the Elusive Catalytic Activity of Vertebrate Class IIa Histone Deacetylases. *Bioorg. Med. Chem. Lett.*, **2008**, *18* [6], 1814–1819.

[12] Mehndiratta, S.; Wang, R.-S.; Huang, H.-L.; Su, C.-J.; Hsu, C.-M.; Wu, Y.-W.; Pan, S.-L.; Liou, J.-P. 4-Indolyl-N-Hydroxyphenylacrylamides as Potent HDAC Class I and IIB Inhibitors in Vitro and in Vivo. *Eur. J. Med. Chem.*, **2017**, *134*, 13–23.

[13] Baroni, M.; Cruciani, G.; Sciabola, S.; Perruccio, F.; Mason, J. S. A Common Reference Framework for Analyzing/Comparing Proteins and Ligands. Fingerprints for Ligands And Proteins [FLAP]: Theory and Application. *J. Chem. Inf. Model.*, **2007**, *47* [2], 279–294.

[14] Poli, G.; Tuccinardi, T.; Rizzolio, F.; Caligiuri, I.; Botta, L.; Granchi, C.; Ortore, G.; Minutolo, F.; Schenone, S.; Martinelli, A. Identification of New Fyn Kinase Inhibitors Using a FLAP-Based Approach. *J. Chem. Inf. Model.*, **2013**, *53* [10], 2538–2547.

[15] Gaulton, A.; Hersey, A.; Nowotka, M.; Bento, A.P.; Chambers, J.; Mendez, D.; Mutowo, P.; Atkinson, F.; Bellis, L.J.; Cibrián-Uhalte, E.; Davies, M.; Dedman, N.; Karlsson, A.; Magariños, M.P.; Overington, J.P.; Papadatos, G.; Smit, I.; Leach, A.R The ChEMBL Database in 2017. *Nucleic Acids Res.*, **2017**, *45* [D1], D945–D954.

[16] Gupta, N.; Pandya, P.; Verma, S. Computational Predictions for Multi-Target Drug Design. In *Multi-Target Drug Design Using Chem-Bioinformatic Approaches. Methods in Pharmacology and Toxicology*; Humana Press, New York, NY, **2018**; pp 27–50.

[17] Berman, H.M.; Westbrook, J.; Feng, Z.; Gilliland, G.; Bhat, T.N.; Weissig, H.; Shindyalov, I.N.; Bourne, P.E. The Protein Data Bank. *Nucleic Acids Res.*, **2000**, *28*, 235−242.

[18] Bottomley, M. J.; Lo Surdo, P.; Di Giovine, P.; Cirillo, A.; Scarpelli, R.; Ferrigno, F.; Jones, P.; Neddermann, P.; De Francesco, R.; Steinkühler, C.; Gallinari, P.; Carfí, A. Structural and Functional Analysis of the Human HDAC4 Catalytic Domain Reveals a Regulatory Structural Zinc-Binding Domain. *J. Biol. Chem.*, **2008**, *283* [39], 26694–26704.

[19] Bürli, R. W.; Luckhurst, C. A.; Aziz, O.; Matthews, K.L.; Yates, D.; Lyons, K.A.; Beconi, M.; McAllister, G.; Breccia, P.; Stott, A.J.; D. Penrose, S.D.; Wall, M.; Lamers, M; Leonard, P.; Müller, I.; Richardson, C.M.; Jarvis, R.; Stones, L.; Hughes, S.; Wishart, G.; Haughan, W.A.; O'Connell, C.; Mead, T.; McNeil, H.; Vann, J.; Mangette, J.; Maillard, M.; Beaumont, V.; Munoz-Sanjuan, I.; Dominguez, C. Design, Synthesis, and Biological Evaluation of Potent and Selective Class IIa Histone Deacetylase [HDAC] Inhibitors as a Potential Therapy for Huntington's Disease. *J. Med. Chem.*, **2013**, *56* [24], 9934–9954.

[20] Luckhurst, C.A.; Breccia, P.; Stott, A.J.; Aziz, O.; Birch, H. L.; Bürli, R. W.; Hughes, S.J.; Jarvis, R.E.; Lamers, M.; Leonard, P.M.; Matthews, K.L.; McAllister, G; Pollack, S.; Saville-Stones, E.; Wishart, G.; Yates, D.; Dominguez, C. Potent, Selective, and CNS-Penetrant Tetrasubstituted Cyclopropane Class IIa Histone Deacetylase [HDAC] Inhibitors. *ACS Med. Chem. Lett.*, **2016**, *7* [1], 34–39.

[21] Somoza, J.R.; Skene, R.J.; Katz, B.A.; Mol, C.; Ho, J.D.; Jennings, A.J.; Luong, C.; Arvai, A.; Buggy, J.J.; Chi, E.; Tang, J.; Sang, B.-C.; Verner, E.; Wynands, R.; Leahy, E.M.; Dougan, D.R.; Snell, G.; Navre, M.; Knuth, M.W.; Swanson, R.V.; McRee, D.E.; Tari, L.W. Structural Snapshots of Human HDAC8 Provide Insights into the Class I Histone Deacetylases. *Structure*, **2004**, *12* [7], 1325–1334.

[22] Dowling, D.P.; Gantt, S.L.; Gattis, S.G.; Fierke, C.A.; Christianson, D.W. Structural Studies of Human Histone Deacetylase 8 and Its Site-Specific Variants Complexed with Substrate and Inhibitors. *Biochemistry*, **2008**, *47* [51], 13554–13563.

[23] Watson, P.J.; Millard, C.J.; Riley, A.M.; Robertson, N.S.; Wright, L.C.; Godage, H.Y.; Cowley, S.M.; Jamieson, A.G.; Potter, B.V.L.; Schwabe, J.W.R. Insights into the Activation Mechanism of Class I HDAC Complexes by Inositol Phosphates. *Nat. Commun.*, **2016**, *7*, 11262.

[24] Lauffer, B.E.L.; Mintzer, R.; Fong, R.; Mukund, S.; Tam, C.; Zilberleyb, I.; Flicke, B.; Ritscher, A.; Fedorowicz, G.; Vallero, R.; Ortwine, D.F.; Gunzner, J.; Modrusan, Z.; Neumann, L.; Koth, C.M.; Lupardus, P.J.; Kaminker, J.S.; Heise, C.E.; Steiner, P. Histone Deacetylase [HDAC] Inhibitor Kinetic Rate Constants Correlate with Cellular Histone Acetylation but Not Transcription and Cell Viability. *J. Biol. Chem.*, **2013**, *288* [37], 26926–26943.

[25] Hai, Y.; Christianson, D.W. Histone Deacetylase 6 Structure and Molecular Basis of Catalysis and Inhibition. *Nat. Chem. Biol.*, **2016**, *12* [9], 741–747.

[26] Schuetz, A.; Min, J.; Allali-Hassani, A.; Schapira, M.; Shuen, M.; Loppnau, P.; Mazitschek, R.; Kwiatkowski, N. P.; Lewis, T. A.; Maglathin, R. L.; McLean, T.H.; Bochkarev, A.; Plotnikov, A.N.; Vedadi, M.; Arrowsmith, C.H. Human HDAC7 Harbors a Class IIa Histone Deacetylase-Specific Zinc Binding Motif and Cryptic Deacetylase Activity. *J. Biol. Chem.*, **2008**, *283* [17], 11355–11363.

[27] Verdonk, M.L.; Cole, J. C.; Hartshorn, M.J.; Murray, C.W.; Taylor, R.D. Improved Protein-Ligand Docking Using GOLD. *Proteins Struct. Funct. Bioinforma.*, **2003**, *52* [4], 609–623. [28] Schrödinger Inc. Macromodel. Portland, OR 2009.

[29] Watson, P.J.; Fairall, L.; Santos, G.M.; Schwabe, J.W.R. Structure of HDAC3 Bound to Co-Repressor and Inositol Tetraphosphate. *Nature*, **2012**, *481* [7381], 335–340.

[30] OpenEye Scientific Software. I. OEChem. Santa Fe, NM, USA **2010**.

[31] Kastenholz, M. A.; Pastor, M.; Cruciani, G.; Haaksma, E.E J.; Fox, T. GRID/CPCA: A New Computational Tool To Design Selective Ligands. *J. Med. Chem.,* **2000**, *43* [16], 3033–3044.

[32] Cross, S.; Baroni, M.; Goracci, L.; Cruciani, G. GRID-Based Three-Dimensional Pharmacophores I: FLAPpharm, a Novel Approach for Pharmacophore Elucidation. *J. Chem. Inf. Model.,* **2012**, *52* [10], 2587–2598.

[33] Ragno, R.; Simeoni, S.; Valente, S.; Massa, S.; Mai, A. 3-D QSAR Studies on Histone Deacetylase Inhibitors. A GOLPE/GRID Approach on Different Series of Compounds. *J. Chem. Inf. Model.,* **2006**, *46* [3], 1420–1430.

[34] Case, D. A.; Berryman, J. T.; Betz, R. M.; Cerutti, D. S.; Cheatham, T.E.I.; Darden, T.A.; Duke, R.E.; Giese, T.J.; Gohlke, H.; Goetz, A.W.; Gusarov, S.; Homeyer, N.; Janowski, P.; Kaus, J.; Kolossváry, I.; Kovalenko, A.; Lee, T.S.; LeGrand, S.; Luchko, T.; Luo, R.; Madej, B.; Merz, K.M.; Paesani, F.; Roe, D.R.; Roitberg, A.; Sagui, C.; Salomon-Ferrer, R.; Seabra, G.; Simmerling, C.L.; Smith, W.; Swails, J.; Walker, R.C.; Wang, J.; Wolf, R.M.; Wu, X.; Kollman, P. A. AMBER, Version 14. University of California: San Francisco, CA, **2015**.

[35] Roe, D.R.; Cheatham, T.E. 3rd. PTRAJ and CPPTRAJ: Software for Processing and Analysis of Molecular Dynamics Trajectory Data. *J. Chem. Theory Comput.*, **2013**, *9*, 3084−3095.

[36] Granchi, C.; Rizzolio, F.; Palazzolo, S.; Carmignani, S.; Macchia, M.; Saccomanni, G.; Manera, C.; Martinelli, A.; Minutolo, F.; Tuccinardi, T. Structural Optimization of 4-Chlorobenzoylpiperidine Derivatives for the Development of Potent, Reversible, and Selective Monoacylglycerol Lipase [MAGL] Inhibitors. *J. Med. Chem.,* **2016**, *59* [22], 10299–10314.

[37] Roberti, A.; Rizzolio, F.; Lucchetti, C.; de Leval, L.; Giordano, A. Ubiquitin-Mediated Protein Degradation and Methylation-Induced Gene Silencing Cooperate in the Inactivation of the INK4/ARF Locus in Burkitt Lymphoma Cell Lines. *Cell Cycle*, **2011**, *10*, 127−134.

[38] Green, M.; Sambrook, J. *Molecular Cloning: A Laboratory Manual*, 5th Ed.; Cold Spring Harbor Laboratory Press: NY, **2012**.

[39] Tuccinardi, T.; Poli, G.; Romboli, V.; Giordano, A.; Martinelli, A. Extensive Consensus Docking Evaluation for Ligand Pose Prediction and Virtual Screening Studies. *J. Chem. Inf. Model.,* **2014**, *54* [10], 2980–2986.

[40] Tuccinardi, T.; Poli, G.; Dell'Agnello, M.; Granchi, C.; Minutolo, F.; Martinelli, A. Receptor-Based Virtual Screening Evaluation for the Identification of Estrogen Receptor β Ligands. *J. Enzyme Inhib. Med. Chem.,* **2015**, *30* [4], 662–670.

[41] Ortore, G.; Colo, F. Di; Martinelli, A. Docking of Hydroxamic Acids into HDAC1 and HDAC8: A Rationalization of Activity Trends and Selectivities. *J. Chem. Inf. Model.,* **2009**, *49* [12], 2774–2785.

[42] Marques, S. M.; Nuti, E.; Rossello, A.; Supuran, C.T.; Tuccinardi, T.; Martinelli, A.; Santos, M. A. Dual Inhibitors of Matrix Metalloproteinases and Carbonic Anhydrases: Iminodiacetyl-Based Hydroxamate−Benzenesulfonamide Conjugates. *J. Med. Chem.,* **2008**, *51* [24], 7968–7979.

[43] Cai, X.; Zhai, H.-X.; Wang, J.; Forrester, J.; Qu, H.; Yin, L.; Lai, C.-J.; Bao, R.; Qian, C. Discovery of 7-[4-[3-Ethynylphenylamino]-7-Methoxyquinazolin-6-Yloxy]- N -Hydroxyheptanamide [CUDC-101] as a Potent Multi-Acting HDAC, EGFR, and HER2 Inhibitor for the Treatment of Cancer. *J. Med. Chem.,* **2010**, *53* [5], 2000–2009.

[44] Auzzas, L.; Larsson, A.; Matera, R.; Baraldi, A.; Deschênes-Simard, B.; Giannini, G.; Cabri, W.; Battistuzzi, G.; Gallo, G.; Ciacci, A.; Vesci, L.; Pisano, C.; Hanessian, S. Non-Natural Macrocyclic Inhibitors of Histone Deacetylases: Design, Synthesis, and Activity. *J. Med. Chem.,* **2010**, *53* [23], 8387–8399.

[45] Wang, H.; Yu, N.; Chen, D.; Lee, K.C.L.; Lye, P.L.; Chang, J.W.W.; Deng, W.; Ng, M.C.Y.; Lu, T.; Khoo, M. L.; Poulsen, A.; Sangthongpitag, K.; Wu, X.; Hu, C.; Goh, K.C.; Wang, X.; Fang L.; Goh, K.L.; Khng, H.H.; Goh, S.K.; Yeo, P.Y.; Liu, X.; Bonday, Z.; Wood, J.M.; Dymock, B.W.; Ethirajulu, K.; Sun, E.T. Discovery of [2E]-3-{2-Butyl-1-[2-[Diethylamino]Ethyl]-1H-Benzimidazol-5-Yl}-N-Hydroxyacrylamide [SB939], an Orally Active Histone Deacetylase Inhibitor with a Superior Preclinical Profile. *J. Med. Chem.,* **2011**, *54* [13], 4694–4720.

[46] Lee, H.-Y.; Tsai, A.-C.; Chen, M.-C.; Shen, P.-J.; Cheng, Y.-C.; Kuo, C.-C.; Pan, S.-L.; Liu, Y.-M.; Liu, J.-F.; Yeh, T.-K.; Wang, J.-C.; Chang, C.-Y-; Chang,J.-Y.; Liou, J.-P. Azaindolylsulfonamides, with a More Selective Inhibitory Effect on Histone Deacetylase 6 Activity, Exhibit Antitumor Activity in Colorectal Cancer HCT116 Cells. *J. Med. Chem.,* **2014**, *57* [10], 4009–4022.

[47] The Leukemia and Lymphoma Society. A Phase 1/2, Open-Label, Multicenter Study of ACY-1215 Administered Orally as Monotherapy and in Combination With Bortezomib and Dexamethasone for the Treatment of Relapsed or Relapsed/Refractory Multiple Myeloma. In: ClinicalTrials.gov [Internet]. Bethesda (MD): U.S. National Library of Medicine.2000. Available from: https://clinicaltrials.gov/ct2/show/NCT01323751.

[48] Carrillo, A.K.; Guiguemde, W.A.; Guy, R.K. Evaluation of Histone Deacetylase Inhibitors [HDACi] as Therapeutic Leads for Human African Trypanosomiasis [HAT]. *Bioorg. Med. Chem.,* **2015**, *23* [16], 5151–5155.

[49] Kozlov, M.V.; Kleymenova, A.A.; Romanova, L.I.; Konduktorov, K.A.; Kamarova, K.A.; Smirnova, O.A.; Prassolov, V.S.; Kochetkov, S.N. Pyridine Hydroxamic Acids Are Specific Anti-HCV Agents Affecting HDAC6. *Bioorg. Med. Chem. Lett.,* **2015**, *25* [11], 2382–2385.

[50] TetraLogic Pharmaceuticals. Safety, Pharmacodynamics (PD), Pharmacokinetics (PK) Study of SHP141 in 1A, 1B, or 2A Cutaneous T-Cell Lymphoma (CTCL). In: ClinicalTrials.gov [Internet]. Bethesda (MD): U.S. National Library of Medicine, **2000**. Available from: https://clinicaltrials.gov/ct2/show/NCT01433731.

[51] Kalin, J.H.; Bergman, J.A. Development and

Therapeutic Implications of Selective Histone Deacetylase 6 Inhibitors. *J. Med. Chem.,* **2013**, *56* [16], 6297–6313.

[52] Andersen JA. Benurestat, a Urease Inhibitor for the Therapy of Infected Ureolysis. *Invest Urol.,* **1975**, *12*, 381–386.

[53] Tuccinardi, T.; Ortore, G.; Santos, M.A.; Marques, S.M.; Nuti, E.; Rossello, A.; Martinelli, A. Multitemplate Alignment Method for the Development of a Reliable 3D-QSAR Model for the Analysis of MMP3 Inhibitors. *J. Chem. Inf. Model.,* **2009**, *49* [7], 1715–1724.

[54] Wang, Y.; Yang, L.; Hou, J.; Zou, Q.; Gao, Q.; Yao, W.; Yao, Q.; Zhang, J. Hierarchical Virtual Screening of the Dual MMP-2/HDAC-6 Inhibitors from Natural Products Based on Pharmacophore Models and Molecular Docking. *J. Biomol. Struct. Dyn.,* **2018**, 1–22.

[55] Goracci, L.; Deschamps, N.; Randazzo, G. M.; Petit, C.; Dos Santos Passos, C.; Carrupt, P.-A.; Simões-Pires, C.; Nurisso, A. A Rational Approach for the Identification of Non-Hydroxamate HDAC6-Selective Inhibitors. *Sci. Rep.,* **2016**, *6* [1], 29086.

[56]Auerbach, S.S.; Svoboda, D. DrugMatrix https://ntp.niehs.nih.gov/results/drugmatrix/index.html.

[57] Daina, A.; Michielin, O.; Zoete, V. SwissADME: A Free Web Tool to Evaluate Pharmacokinetics, Drug-Likeness and Medicinal Chemistry Friendliness of Small Molecules. *Sci. Rep.*, **2017**, *7* [1], 42717.

[58] Gelpi, J.; Hospital, A.; Goñi, R.; Orozco, M. Molecular Dynamics Simulations: Advances and Applications. *Adv. Appl. Bioinforma. Chem.,* **2015**, 37.

[59] Ortore, G.; Tuccinardi, T.; Bertini, S.; Martinelli, A. A Theoretical Study To Investigate D2DAR/D4DAR Selectivity: Receptor Modeling and Molecular Docking of Dopaminergic Ligands. *J. Med. Chem.,* **2006**, *49* [4], 1397–1407.

[60] Tuccinardi, T.; Ortore, G.; Manera, C.; Saccomanni, G.; Martinelli, A. Adenosine Receptor Modelling. A1/A2a Selectivity. *Eur. J. Med. Chem.,* **2006**, *41* [3], 321–329.

[61]Liu, K.; Watanabe, E.; Kokubo, H. Exploring the Stability of Ligand Binding Modes to Proteins by Molecular Dynamics Simulations. *J. Comput. Aided. Mol. Des.,* **2017**, *31* [2], 201–211.

[62] Wang, S.-H.; Wang, S.-F.; Xuan, W.; Zeng, Z.-H.; Jin, J.-Y.; Ma, J.; Tian, G. R. Nitro as a Novel Zinc-Binding Group in the Inhibition of Carboxypeptidase A. *Bioorg. Med. Chem.,* **2008**, *16* [7], 3596–3601.

[63] Wang, H.; Xiao, H.; Liu, N.; Zhang, B.; Shi, Q. Three New Compounds Derived from Nitrofurantoin: X-Ray Structures and Hirshfeld Surface Analyses. *Open J. Inorg. Chem.,* **2015**, *5*, 63–73.

[64] Sączewski, F.; Stencel, A.; Bieńczak, A. M.; Langowska, K. A.; Michaelis, M.; Werel, W.; Hałasa, R.; Reszka, P.; Bednarski, P. J. Structure–Activity Relationships of Novel Heteroaryl-Acrylonitriles as Cytotoxic and Antibacterial Agents. *Eur. J. Med. Chem.,* **2008**, *43* [9], 1847–1857.

[65] Andrade, J.K.F.; Souza, M.I.F.; Gomes Filho, M.A.; Silva, D.M.F.; Barros, A.L.S.; Rodrigues, M.D.; Silva, P. B. N.; Nascimento, S.C.; Aguiar, J.S.; Brondani, D.J.; Militão, G.C.G.; Silva, T.G. N-Pentyl-Nitrofurantoin Induces Apoptosis in HL-60 Leukemia Cell Line by Upregulating BAX and Downregulating BCL-XL Gene Expression. *Pharmacol. Reports,* **2016**, *68* [5], 1046–1053.

[66] Nelson, E.A.; Walker, S.R.; Kepich, A.; Gashin, L.B.; Hideshima, T.; Ikeda, H.; Chauhan, D.; Anderson, K.C.; Frank, D.A. Nifuroxazide Inhibits Survival of Multiple Myeloma Cells by Directly Inhibiting STAT3. *Blood,* **2008**, *112* [13], 5095–5102.

[67] Gupta, M.; Han, J.J.; Stenson, M.; Wellik, L.; Witzig, T.E. Regulation of STAT3 by Histone Deacetylase-3 in Diffuse Large B-Cell Lymphoma: Implications for Therapy. *Leukemia,* **2012**, *26* (6], 1356–1364.